ACS APPLIED ENERGY MATERIALS
Cite This: ACS Appl. Energy Mater. 2019, 2, 8580−8586
Article
www.acsaem.org

Water-Assisted Growth of Cobalt Oxide and Cobalt Hydroxide Overlayers on the $Pt_3Co(111)$ Surface

Jeongjin Kim,[†] Won Hui Doh,[†] Youngjae Kim,[†,§] Ki-Jeong Kim,[‡] and Jeong Young Park*[,†,§]

[†]Center for Nanomaterials and Chemical Reactions, Institute for Basic Science (IBS), Daejeon 34141, Republic of Korea
[‡]Beamline Research Division, Pohang Accelerator Laboratory (PAL), Pohang 37673, Republic of Korea
[§]Department of Chemistry, Korea Advanced Institute of Science and Technology (KAIST), Daejeon 34141, Republic of Korea

Supporting Information

ABSTRACT: Bimetallic platinum−cobalt (Pt−Co) catalysts have highly enhanced performance for the oxygen reduction reaction (ORR), where this peculiar surface alloy structure contributes to efficient energy conversion processes. However, the detailed catalytic reaction steps and adsorbate-driven interactions on the surface morphology under practical operating conditions are still unclear. Here, we report the water-assisted surface reconstruction of the bimetallic $Pt_3Co(111)$ surface using near-ambient pressure scanning tunneling microscopy (NAP-STM) in a humid O_2 environment. The segregated CoO_x clusters are selectively transferred to the Co(II) oxide/hydroxide layer at 0.1 Torr of H_2O/O_2 gas mixture at elevated temperature. In contrast, this drastic phase transition is limited and dependent on the partial pressure of water because the nanoscale CoO islands are formed with 0.1 Torr of the N_2/O_2 gas mixture. Synchrotron radiation in-situ X-ray photoelectron spectroscopy measurements also support the water-assisted evolution of the $Co(OH)_2$ species. These morphologic modulations not only explain the surface degradation process of the bimetallic Pt−Co catalysts but also indicate the active formation of CoO_x/CoOOH intermediates during energy conversion.

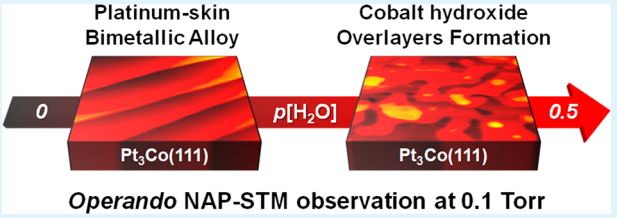

KEYWORDS: *Pt−Co catalyst, water/solid interface, surface reconstruction, operando observation, energy conversion*

1. INTRODUCTION

Novel utilization of renewable and clean energy production has been at the top of international agendas for decades to solve the steep depletion of fossil fuel sources.[1,2] Among the various solutions, a promising eco-friendly alternative is the direct conversion of chemical energy to electrical energy in a fuel cell using Pt electrocatalysts. However, it is a challenge to overcome practical issues like the overpotential of the Pt cathode in the rate-limiting step of the oxygen reduction reaction ($O_2 + 4H^+ + 4e^- \rightarrow 2H_2O$, $E_0 = +1.23$ V vs reversible hydrogen electrode (RHE))[3] and the high cost of Pt, which is especially a hurdle for large-scale operations.[4] Thereby, extensive studies searching for Pt substitutes while enhancing the efficiency of energy production deal with the rational design of electrocatalysts. In particular, Pt-based bimetallic alloys successfully meet the requirements to replace Pt (e.g., designs of Co- or Ni-alloyed Pt catalysts exemplify a superior catalyst with respect to the volcano plot of energy conversion).[5−9] Tailored layers in the surface of Pt-based bimetallic catalysts have unique electronic structures that facilitate beneficial molecular interactions via Sabatier's principle for enhancing catalytic activity.[10] Theoretically, a shift of the d-band near the Fermi edge in the electronic structure of Pt-based bimetallic materials by alloyed 3d transition metal (TM) components can make fine adjustments to the chemical bonding states on the surface, which conclusively explains the origin of previous important benchmark reports of Pt-TM and electrocatalysis.[5,11] Nonetheless, the very large mass and charge transfers that occur during molecular interactions complicate the oxidation/reduction reactions at the liquid/solid interface and are not yet fully understood. The degradation process for bimetallic catalysts in cyclic activity measurements has been investigated to understand the relationship between catalyst morphology and reactivity; these details have been much debated.[12−14] Gaining a fundamental understanding of molecular behavior on the active sites of transient catalyst morphologies under realistic conditions requires in-situ microscopic and spectroscopic surface techniques that are operable at elevated pressure and temperature.[15,16]

In this study, we reveal a phase transition of the morphology of the $Pt_3Co(111)$ surface using near-ambient pressure scanning tunneling microscopy (NAP-STM) in a humid O_2 environment. The prepared Pt-skin topmost layer of the Pt−Co surface is gradually covered with partially oxidized CoO_x clusters that result from surface segregation of subsurface Co atoms under oxidation conditions. We show that the partial pressure of water is a crucial factor for determining the

Received: July 31, 2019
Accepted: November 21, 2019
Published: November 21, 2019

DOI: 10.1021/acsaem.9b01484
ACS Appl. Energy Mater. 2019, 2, 8580−8586

consecutive restructuring process. This water-assisted surface reconstruction makes large multilayered holes and pits in the Co(II) oxide/hydroxide structures, while the segregated CoO_x clusters grow to CoO islands on the $Pt_3Co(111)$ surface when exposed to O_2. Synchrotron radiation in-situ X-ray photoelectron spectroscopy (XPS) was used to identify the oxidation states of the Co before and after surface segregation. Our experiments at more realistic conditions explain the surface degradation process of the model Pt−Co bimetallic catalyst by water molecule interactions at increased thermodynamic potentials.[17−19]

2. EXPERIMENTAL PROCEDURES

2.1. Operando Direct Observations Using NAP-STM. Direct observation images were taken by using a reaction cell (15 mL) integrated STM scanner (Aarhus STM 150 NAP, SPECS GmbH) in an ultrahigh-vacuum (UHV) chamber (base pressure: 1×10^{-10} Torr) that is connected to a high-purity (99.999%) multigas delivery manifold system. Each STM image was recorded in constant current mode where the tunneling condition is denoted as V_s (sample bias voltage) with I_t (tunneling current).

2.2. Synchrotron Radiation in-Situ XPS Measurements. Photoemission core-level electron transition signals were acquired at the HR-PES II end-station of the 10A2 beamline with an undulating X-ray radiation source in top-up mode at the Pohang Accelerator Laboratory (PAL) in the Republic of Korea. XPS measurements were performed in an UHV chamber (base pressure: 4×10^{-11} Torr) that is equipped with a hemispherical electron analyzer (SES200, Scienta). The X-ray beam incidence angle was selectively adjusted to the sample surface (takeoff angle of 30° for surface-sensitive and 90° for subsurface-sensitive) in the measurements. Photoelectron spectra were recorded with a step of 0.05 eV and a pass energy of 20 eV. Each acquired spectrum binding energy was calibrated to the Fermi edge of the clean sample at each selected photon energy. The collected XP spectra were analyzed by using a commercially available software package (CasaXPS 2.3.19). The binding energy calibrated spectra were subtracted by using a Shirley-type background before the curve-fitting procedure. The O 1s core-level spectra were deconvoluted with widely used fitting parameters with a Gaussian (70%) and Lorentzian (30%) mixed function.

2.3. Preparation of Single-Crystal $Pt_3Co(111)$ Surface. A polished $Pt_3Co(111)$ sample with a cut accuracy <0.1° was purchased from Mateck GmbH (Germany) and pretreated by using cyclic Ar^+ ion-bombardment sputtering of 1000 eV at 1×10^{-5} Torr for 20 min, followed by UHV annealing at 1100 K for 5 min. This straightforward procedure was repeated until obtaining a monolayer Pt-skin-covered $Pt_3Co(111)$ surface without any contaminants in each separate analysis system. Detailed experimental procedures are described elsewhere.[20,21]

3. RESULTS AND DISCUSSION

The prepared $Pt_3Co(111)$ surface image exhibits a typical step-terrace structure at 300 K in UHV (Figure 1a). Each of the measured step heights is 2.3 Å, and the nearest-neighbor distance is ∼2.8 Å on the terrace (inset of Figure 1a). The indicated hexagonal spots (white dotted line) in the Fast-Fourier transform (FFT) image confirm the (111) facet of the Pt atom arrays on the locally magnified terrace area (Figure S1 in the Supporting Information), which means that the pretreated clean $Pt_3Co(111)$ surface consists of an upper Pt skin with Pt−Co alloyed subsurface layers.[22,23]

The observed Pt-skin/$Pt_3Co(111)$ surface is suddenly altered depending on the surface interactions with the surrounding adsorbate molecules. In Figure 1b, the operando NAP-STM image shows bright nanoislands (indicated by arrows) with dark pits along the deformed step-terrace

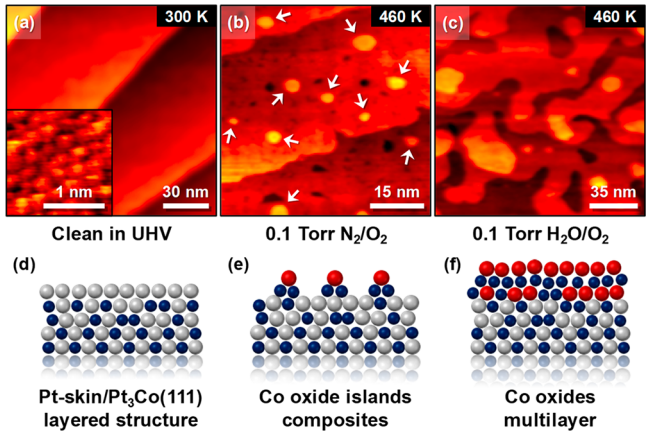

Figure 1. NAP-STM images of the $Pt_3Co(111)$ under different measurement conditions with corresponding schematics. (a) Clean at UHV and 300 K [V_s = 1.25 V; I_t = 0.19 nA] with an enlarged atom-resolved Pt-skin STM image (inset) [V_s = 0.37 V; I_t = 0.13 nA], (b) Co oxide nanoisland evolution with 0.1 Torr of N_2/O_2 gas mixture at 460 K [V_s = 1.28 V; I_t = 0.29 nA], and (c) Co oxide multilayer formation with 0.1 Torr of the H_2O/O_2 gas mixture at 460 K [V_s = 1.10 V; I_t = 0.18 nA]. Schematic models of the (d) Pt-skin/$Pt_3Co(111)$ layer, (e) Co oxide island composites, and (f) multilayer Co oxide structure (side view). The colors for each atom indicate Pt (light gray), Co (royal blue), and O (red) in the schematic models.

structures during the dry oxidation process (0.1 Torr of N_2/O_2 1:1 ratio gas mixture) at 460 K. Representative line profiles (Figure S2) indicate that the apparent height of the nanoislands is close to 1.6 Å, and the reconstructed step heights on the observed surface are in the range 1.4−1.9 Å. The nanoislands are similar to an earlier report of stoichiometric CoO islands on an oxidized Co/Au(111) surface.[24] Furthermore, the randomly formed pits on the terraces have height profiles of 1.0−2.1 Å during the evolution of nanoclusters and nanoislands, where the observed deformation of the Pt-skin/$Pt_3Co(111)$ surface is certainly triggered by subsurface Co atom segregation under dry oxidation conditions. However, we observed a widely formed, winding layered structure when in a humid O_2 environment (0.1 Torr of H_2O/O_2 1:1 ratio gas mixture) at 460 K (Figure 1c). The reconstructed morphology has an apparent height of 5.0 Å between the lowest valley and the highest peak in the measured line profile (Figure S3). The nanoislands on the observed image seem to have discrete step edge structures, which provides evidence of reconstructed metal−oxide interface formation with three different layers of 1.7 Å average step height. This unusual picture obviously differs from the dry oxidation process. The formation of an adsorbate-driven layered structure is assisted by the surrounding water molecules during oxidation of the segregated Co atoms on the $Pt_3Co(111)$ surface at the increased thermodynamic surface potential under reaction conditions. Based on our direct observations, schematics of the bimetallic Pt−Co compositions on the surface are proposed as Pt-skin/$Pt_3Co(111)$, Co oxide island composites, and Co oxide multilayer structures, as illustrated in Figure 1d−f.

Figure 2a−d shows the characteristic processes of water-induced Co oxide evolution on the $Pt_3Co(111)$ surface under operando conditions. Under the humid O_2 conditions, most of the terraces were covered with varying sizes (4−10 nm) of nanocluster networks at 370 K, as shown in Figure 2a.

DOI: 10.1021/acsaem.9b01484
ACS Appl. Energy Mater. 2019, 2, 8580−8586

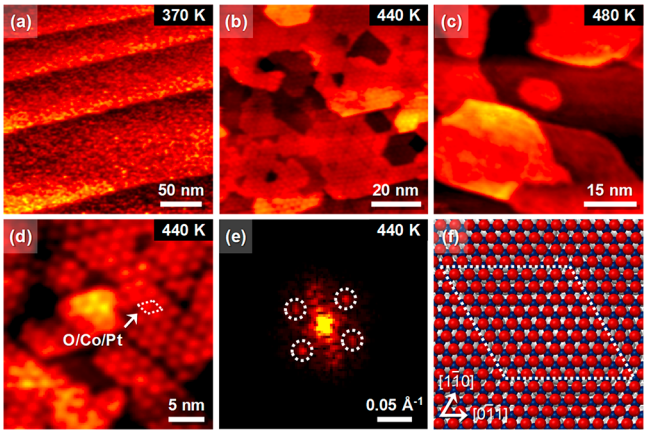

Figure 2. Operando NAP-STM images with 0.1 Torr of H_2O/O_2 gas mixture on the $Pt_3Co(111)$ surface at temperatures of (a) 370 K [V_s = 1.00 V; I_t = 0.11 nA], (b) 440 K [V_s = 1.10 V; I_t = 0.19 nA], and (c) 480 K [V_s = 1.10 V; I_t = 0.19 nA]. (d) A local magnified operando NAP-STM image at 440 K [V_s = 1.10 V; I_t = 0.23 nA]. (e) Two-dimensional FFT image of (d). (f) Atomistic ball model of the O/Co/Pt layered structure (red: O; royal blue: Co; light gray: Pt).

Subsurface Co atoms could selectively segregate onto the topmost layer when surrounded by O_2 molecules, which was also observed in previous reports of Pt-based bimetallic catalysts.[23,25] The chemical potential of the reactive molecules influence the morphology, which implies that the control of pressure and temperature in the surrounding environment would lead to morphological changes via surface reconstruction or restructuring.[26] These morphological changes originate from the inherent lattice mismatch between the Pt and 3d-TM of the bimetallic alloy materials. For instance, Pt_3Co has a 2% reduced fcc lattice constant with a segregation energy of −0.61 eV compared with Pt in a theoretically optimized model structure.[27] The dissociated oxygen pulls the subsurface Co atoms onto the topmost layer, and the segregated CoO_x nanoclusters are spontaneously formed on the $Pt_3Co(111)$ surface via strain and ligand effects.[28,29] The oxygen-induced phase separation of $Pt_3Co(111)$ and segregated CoO_x nanocluster oxidation would be followed by the thermodynamic relation at a given temperature and pressure.[30] For example, selective Co segregation on the $Pt_3Co(111)$ surface is easily observed even at 300 K in 1 Torr of O_2 compared with an O_2 pressure 1/20th of that (Figure S4). This subsurface Co atom segregation process occurs on the $Pt_3Co(111)$ under both dry and humid oxidation conditions at temperatures under 400 K, regardless of the partial pressure of water.

Surprisingly, the observed surface structure has an abrupt phase transition stage at temperatures above 400 K during humid oxidation. The reconstructed surface shows broken steps and holes with periodic arrays at 440 K (Figure 2b). Finally, the evolved layers combined with each other at 480 K (Figure 2c) to make an ultrathin Co oxide multilayer on the

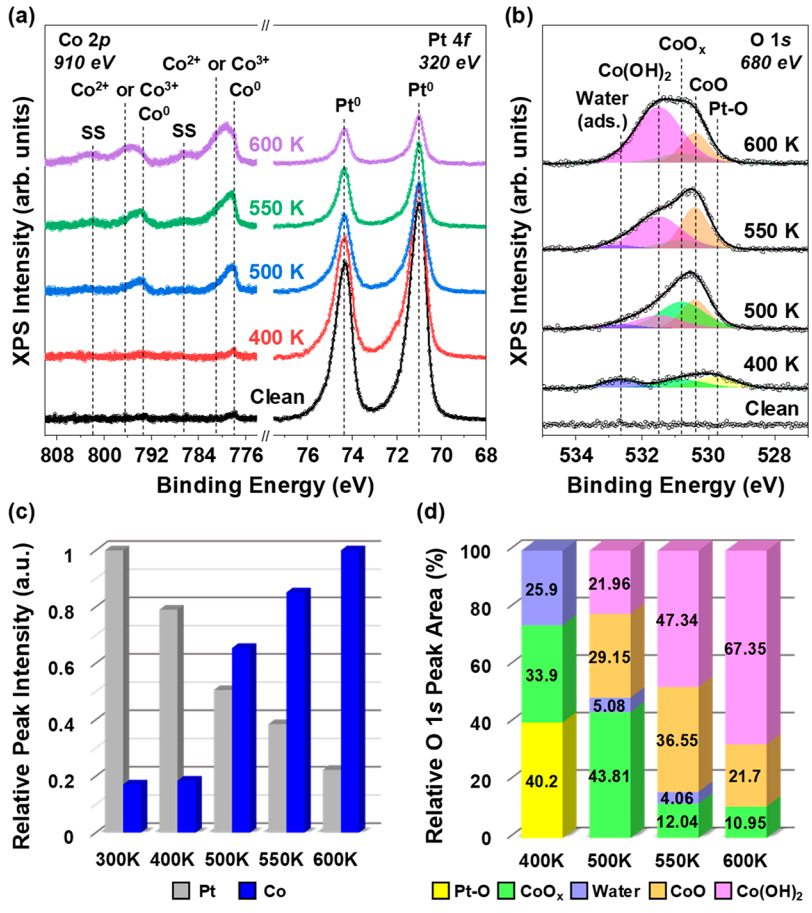

Figure 3. Synchrotron radiation in-situ XPS measurements on the $Pt_3Co(111)$ surface with 2×10^{-6} Torr of H_2O/O_2 (1:1 ratio) gas mixture and at elevated temperature. Comparison of the core-level XP spectra of (a) Co 2p and Pt 4f and (b) O 1s. (c) Relative peak intensity histogram of the Pt and Co core-level XP spectra. (d) Stacked column plots of the relative peak areas from the O 1s core-level XP spectra.

DOI: 10.1021/acsaem.9b01484
ACS Appl. Energy Mater. 2019, 2, 8580−8586

surface. In Figure 2d, the enlarged image taken during operando observations at 440 K clearly shows the moiré pattern fragments of the layered structure with a periodicity of 2.4 nm. As shown in Figure 2e, the FFT results in Figure 2d also provide strong evidence (white dotted circles) of the presented periodicity. This observed structure matches a previously proposed superstructure of "O/Co/Pt" (see schematic illustration in Figure 2f).[31] Thus, the water-assisted surface reconstruction has a large discrepancy from the trend seen with dry oxidation on the $Pt_3Co(111)$ surface. According to a kinetic Monte Carlo (kMC) simulation, the selectively dissolved components organize porosities on the terraces such that the nonequilibrium dealloying behavior of the external holes and pits occur at the liquid/alloy interface.[32] Pourbaix diagrams also describe how the Co−H_2O system may form Co_3O_4, $Co(OH)_2$, $Co(OH)_3$, and CoOOH in neutral pH at equilibrium potentials.[33] Water-induced agglomeration of the CoO_x clusters could lead to a wide range of surface reconstruction. The revealed water-assisted Co oxide multilayer formation on the $Pt_3Co(111)$ is analogous to two-dimensional $Co(OH)_2$/CoOOH and Co oxide island structures on Au catalysts.[34,35] As described above, observations of the evolved morphology show a considerable discrepancy between the structural formation with respect to the partial pressure of water. Notwithstanding these valuable results, confirmation of the chemical binding information is key to investigating the origin of the specific compositions on the layered Pt−Co alloy surface.

To clarify the chemical species information, we performed in-situ synchrotron radiation XPS measurements on the $Pt_3Co(111)$ surface with 2×10^{-6} Torr of water and an O_2 gas mixture (1:1 ratio) with increasing temperature. We selected photon energies of 320 eV for Pt 4f, 680 eV for O 1s, and 910 eV for Co 2p core-level photoelectron spectra. At a takeoff angle of 30° against the hemispherical electron analyzer, we could actually collect surface-sensitive chemical binding information from the surface in the range of 1−2 nm; experimental apparatus adjustments are particularly important to interpret the adsorbed molecular water (hydroxyl group coupling of the Co oxide) (Figure S5).[36] As shown in Figure 3a, the core-level spectra of Pt 4f and Co 2p show changes in the relative elemental composition of the Pt and Co on the $Pt_3Co(111)$ surface at elevated temperatures. The absolute intensity of the Pt 4f core-level spectrum gradually decreased with increasing temperature; however, the Co 2p core-level spectrum increased at the same temperature. We identified a shift of the metallic Co (Co^0) peak at 778.2 eV toward to Co^{2+} or Co^{3+} at a binding energy of 780.9 eV with increasing temperature.[37] Moreover, the noticeable shakeup satellite (SS) peak appears at 787.0 eV when at temperatures above 550 K, which confirms the change in oxidation state at 600 K in the XP spectra. According to the literature, synthesized nanomaterials such as CoO, $Co(OH)_2$, CoOOH, and Co_3O_4 show a representative characteristic XP spectral shape such that each chemical species is distinguished by deconvoluted peak positions.[38,39] Notably, a broad satellite peak appears in each analysis result for CoO and $Co(OH)_2$ at binding energies of 786.5 and 786.3 eV, respectively, in the literature. Thus, the observed peak shift at temperatures above 550 K in the measured Co 2p core-level spectra is attributed to a change in the oxidation state ($Co^0 \rightarrow Co^{2+}$). Overall, the acquired chemical species results imply that the pretreated clean Pt-skin/$Pt_3Co(111)$ surface could be selectively oxidized to Co oxides/hydroxide under humid oxidation conditions.

Figure 3b shows the detailed changes in the oxidation state for both the Pt and Co in the simultaneously acquired O 1s spectra. At 400 K, three different characteristic peaks appeared at 529.8, 530.8, and 532.7 eV; they can be assigned to Pt−O (chemisorbed oxygen), partially oxidized nonuniform CoO_x ($0 < x \leq 0.5$) clusters, and coupled water molecules on the CoO_x species, respectively.[23,36] This confirms that the CoO_x segregation phenomenon occurs via dissociated oxygen from the water and O_2 gas mixture on the $Pt_3Co(111)$ surface at 400 K. We note that dissociated water molecules were not found at 300 K, nor on the clean surface (i.e., the dissociated hydroxyl group from the water molecule is selectively adsorbed on the segregated CoO_x networks and not on the Pt atoms). Typically, the adsorption of water molecules on Pt atoms is not favored even at 160 K;[40] however, the partially oxidized CoO_x clusters prefer electrophilic adsorbates, such as dissociated water, to create more stable electron configurations.[41] For instance, the edge sites of CoO actively facilitate water dissociation even at room temperature because the exposed active sites cause dynamic changes in the chemical state on the surface.[34]

Thus, the adsorbed molecular water or the coupled hydroxyl group (−OH) appears at a relatively higher binding energy above 531 eV in the XP spectrum for the metal−oxide system.[42,43] With the acceleration of the humid oxidation process above 500 K, the Pt−O peak disappears, and peaks for the lattice oxygen (CoO) and Co hydroxide [$Co(OH)_2$] species suddenly emerge at 530.4 and 531.5 eV, respectively. Crystallography of the stable Co_3O_4 bulk structure consists of Co^{2+} from tetragonal and Co^{3+} from octahedral sites;[19] however, we could not deconvolute each feature with the ratio of Co^{2+}/Co^{3+} for Co_3O_4 because the segregated amounts of the Co atoms were not sufficient to have a large-scale stable bulk structure. Nevertheless, the peak at 531.5 eV could be assigned to $Co(OH)_2$ at 500 K, except for bulk Co_3O_4 formation, because the simultaneous shift of the primary peak position and the intensity ratio to the SS peak in the acquired Co 2p spectrum were different than the reference results for Co_3O_4 formation.[38,39] The SS peak in the Co 2p spectra originated from complex electron-exchange correlations between the initial and final states of the Co oxides. In molecular orbital (MO) theory, the solution of the wave equation based on quantum mechanics calculations asserts that an electron transition from O 2p to Co 3d contributes to the overlapped peak shapes of the SS species with oxidation states of Co^{2+}.[44]

Therefore, the assignment of the peak for $Co(OH)_2$ is reasonable in the O 1s spectra at elevated temperature. Above 400 K, consumption of the adsorbed −OH group occurs readily during transformation of the intermediate CoOOH; thus, the CoO_x and adsorbed water species simultaneously decreased at 550 K. Eventually, the $Co(OH)_2$ peak has the largest portion of the deconvoluted peak areas in the O 1s spectrum at 600 K. Figure 3c,d aids in the numerical analysis of the XP spectra by providing plots of the histograms. These histograms display the fractional ratio of the Pt and Co elements on the $Pt_3Co(111)$ surface and the trends of the relative peak areas for each Co oxide species at a given time. It shows that the segregated Co changed oxidation states with increasing temperature; in the end, the oxide structure

DOI: 10.1021/acsaem.9b01484
ACS Appl. Energy Mater. 2019, 2, 8580−8586

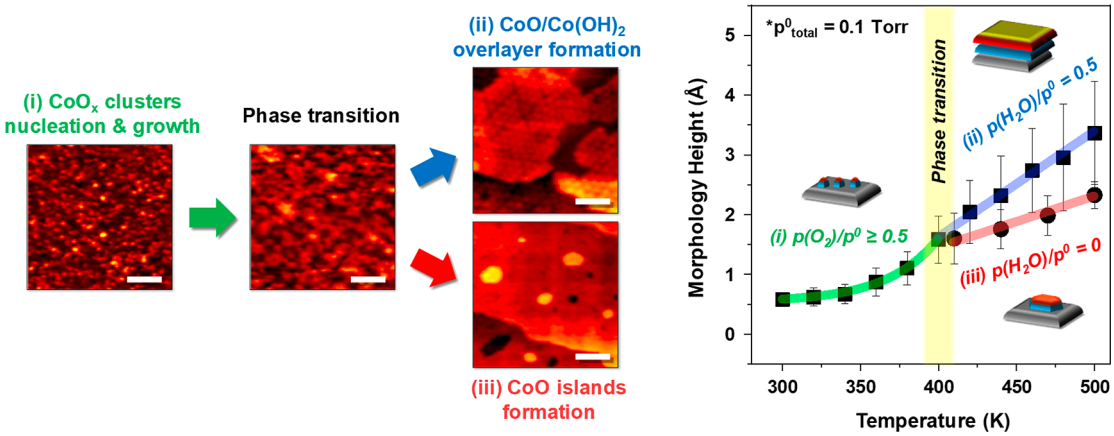

Figure 4. Representative operando NAP-STM images and plot of the measured evolving morphology height on the $Pt_3Co(111)$ surface from NAP-STM images under environmental conditions. Each representative image (scale bar: 10 nm) shows a separate surface reconstruction step in the respective dry and humid oxidation processes at elevated temperature.

consisted of a predominantly $Co(OH)_2$ overlayer on the surface.

Figure 4 displays a statistical plot based on the measured height of the evolving species of CoO_x clusters, CoO islands, and the $CoOOH/Co(OH)_2$ overlayer from the NAP-STM images under operando conditions (p^0_{total} = 0.1 Torr). Oxygen-driven CoO_x segregation occurred almost uniformly along the terraces of the $Pt_3Co(111)$ catalyst, where clusters grew via the Ostwald-ripening process of nucleation and coalescence at elevated temperature. Thus, the agglomerated CoO_x cluster size increased exponentially up to 400 K. A dramatic phase transition began with selective surface reconstruction dependent on whether the −OH group was bound to the networks of nucleated CoO_x. The dry oxidation process $[p(H_2O)/p^0 = 0]$ led to the formation of CoO on the Pt−Co alloy surface where the average height of the nucleated CoO_x islands grew linearly up to 2.3 ± 0.2 Å at 500 K. This increased by 30.4% compared with the morphology height at 410 K, at which temperature the islands corresponded to the CoO structure. In contrast, the humid oxidation process $[p(H_2O)/p^0 = 0.5]$ readily constructs an overlayer structure on the $Pt_3Co(111)$ surface. After the indicated phase transition at 400 K, the $Co(OH)_2$ layer grew epitaxially with increasing temperature. This vigorous reconstruction has a measured morphology height of 3.4 ± 0.9 Å at 500 K, which corresponds to approximately double the measured height of the bilayer CoO island structure.[36] Their measured height profiles indicate wider distributions than that of CoO nanoisland structure. This implies that the observation results in more extreme experimental conditions might have a sub-angstrom-level error scale. However, the variation of average morphology height distribution under humid oxidation conditions was significantly higher than the error scale and could therefore be considered solid evidence of the effect of vapored water molecules. Also, in the results of our operando NAP-STM and in-situ XPS, we did not observe the formation of multilayer CoO or CoOOH structures on the $Pt_3Co(111)$ surface in experimental conditions with dry or humid oxidation. Unlike the nucleation and growth step before the surprising phase transition at 400 K, both dry and humid oxidation promote monotonic growth of islands or overlayers at elevated temperatures. Repeated units of Co−O might make an unfavorable dipole moment during island or layer growth, where the opposing charge polarization between the Co- or O-terminated layers should compensate for one other to stabilize the oxide structure.[45,46]

Thus, the water-assisted adsorbate interactions are not limited to forming surface oxides but can develop an influential ultrathin oxide layer. It follows that the Co oxides may have many oxidation states because of structural flexibility, which explains the potential for novel construction of nanoscale architecture.[18,19] Especially, the evolution of an intermediate CoOOH layer is very important for the direct conversion of energy via the oxygen evolution reaction (OER). This active phase could play an effective role in the four-electron exchange process at liquid/solid interfaces.[47] Moreover, the identified Co oxide and hydroxide overlayers may provide a relaxation pathway for hot carriers through the specified electron transition $[O^{2-}(2p) \rightarrow Co^{3+}(e_g)]$,[48] which could also be used for ultrathin metal−oxide layered devices in industrial energy applications.[49,50]

4. CONCLUSION

The detailed surface phase transition process of a bimetallic $Pt_3Co(111)$ model catalyst has been observed in operando conditions using NAP-STM. Dissociated oxygen with increasing chemical potential energy leads to subsurface Co atoms segregating onto the topmost Pt-skin layer of the $Pt_3Co(111)$ surface. After the segregated CoO_x clusters form, the phase transition step selectively proceeds as a function of water partial pressure. The oxygen-driven nucleated CoO_x networks are spontaneously transformed to an ultrathin $CoO/Co(OH)_2$ overlayer on the $Pt_3Co(111)$ surface by the hydroxylation reaction during the humid oxidation process. We show that in-situ XPS analysis results are consistent with the observed trend of the morphologic changes seen in NAP-STM images where the segregated CoO_x species underwent $Co(OH)_2$ layer formation when exposed to a water and O_2 gas mixture at elevated temperature. These investigations clarify the elementary step of transient Co oxide formation on Pt−Co bimetallic catalyst surfaces during the ORR at an increased chemical potential.

■ ASSOCIATED CONTENT

Supporting Information

The Supporting Information is available free of charge at https://pubs.acs.org/doi/10.1021/acsaem.9b01484.

DOI: 10.1021/acsaem.9b01484
ACS Appl. Energy Mater. 2019, 2, 8580−8586

Figures S1−S5: NAP-STM images with representative line profiles and angle-dependent O 1s core-level XP spectra in a water/O_2 gas mixture (PDF)

AUTHOR INFORMATION

Corresponding Author

*E-mail: jeongypark@kaist.ac.kr.

ORCID

Jeongjin Kim: 0000-0002-3790-1684
Won Hui Doh: 0000-0001-5109-4471
Youngjae Kim: 0000-0003-1679-6093
Ki-Jeong Kim: 0000-0001-9233-3096
Jeong Young Park: 0000-0002-8132-3076

Notes

The authors declare no competing financial interest.

ACKNOWLEDGMENTS

This work was supported by the Institute for Basic Science (IBS) [IBS-R004]. The experiments at PLS-II were supported in part by MSICT and POSTECH and NRF-2018R1D1A1B07048177.

REFERENCES

(1) Somorjai, G. A.; Frei, H.; Park, J. Y. Advancing the Frontiers in Nanocatalysis, Biointerfaces, and Renewable Energy Conversion by Innovations of Surface Techniques. *J. Am. Chem. Soc.* **2009**, *131*, 16589−16605.

(2) Chu, S.; Majumdar, A. Opportunities and challenges for a sustainable energy future. *Nature* **2012**, *488*, 294−303.

(3) Nørskov, J. K.; Rossmeisl, J.; Logadottir, A.; Lindqvist, L.; Kitchin, J. R.; Bligaard, T.; Jónsson, H. Origin of the Overpotential for Oxygen Reduction at a Fuel-Cell Cathode. *J. Phys. Chem. B* **2004**, *108*, 17886−17892.

(4) Morozan, A.; Jousselme, B.; Palacin, S. Low-platinum and platinum-free catalysts for the oxygen reduction reaction at fuel cell cathodes. *Energy Environ. Sci.* **2011**, *4*, 1238−1254.

(5) Stamenkovic, V. R.; Mun, B. S.; Arenz, M.; Mayrhofer, K. J. J.; Lucas, C. A.; Wang, G.; Ross, P. N.; Markovic, N. M. Trends in electrocatalysis on extended and nanoscale Pt-bimetallic alloy surfaces. *Nat. Mater.* **2007**, *6*, 241−247.

(6) Stamenkovic, V. R.; Fowler, B.; Mun, B. S.; Wang, G.; Ross, P. N.; Lucas, C. A.; Marković, N. M. Improved Oxygen Reduction Activity on $Pt_3Ni(111)$ via Increased Surface Site Availability. *Science* **2007**, *315*, 493−497.

(7) Wang, D.; Xin, H. L.; Hovden, R.; Wang, H.; Yu, Y.; Muller, D. A.; DiSalvo, F. J.; Abruña, H. D. Structurally ordered intermetallic platinum−cobalt core−shell nanoparticles with enhanced activity and stability as oxygen reduction electrocatalysts. *Nat. Mater.* **2013**, *12*, 81−87.

(8) Chen, C.; Kang, Y.; Huo, Z.; Zhu, Z.; Huang, W.; Xin, H. L.; Snyder, J. D.; Li, D.; Herron, J. A.; Mavrikakis, M.; Chi, M.; More, K. L.; Li, Y.; Markovic, N. M.; Somorjai, G. A.; Yang, P.; Stamenkovic, V. R. Highly Crystalline Multimetallic Nanoframes with Three-Dimensional Electrocatalytic Surfaces. *Science* **2014**, *343*, 1339−1343.

(9) Gan, L.; Cui, C.; Heggen, M.; Dionigi, F.; Rudi, S.; Strasser, P. Element-specific anisotropic growth of shaped platinum alloy nanocrystals. *Science* **2014**, *346*, 1502−1506.

(10) Medford, A. J.; Vojvodic, A.; Hummelshøj, J. S.; Voss, J.; Abild-Pedersen, F.; Studt, F.; Bligaard, T.; Nilsson, A.; Nørskov, J. K. From the Sabatier principle to a predictive theory of transition-metal heterogeneous catalysis. *J. Catal.* **2015**, *328*, 36−42.

(11) Stephens, I. E. L.; Bondarenko, A. S.; Perez-Alonso, F. J.; Calle-Vallejo, F.; Bech, L.; Johansson, T. P.; Jepsen, A. K.; Frydendal, R.; Knudsen, B. P.; Rossmeisl, J.; Chorkendorff, I. Tuning the Activity of Pt(111) for Oxygen Electroreduction by Subsurface Alloying. *J. Am. Chem. Soc.* **2011**, *133*, 5485−5491.

(12) Mayrhofer, K. J. J.; Hartl, K.; Juhart, V.; Arenz, M. Degradation of Carbon-Supported Pt Bimetallic Nanoparticles by Surface Segregation. *J. Am. Chem. Soc.* **2009**, *131*, 16348−16349.

(13) Yu, Y.; Xin, H. L.; Hovden, R.; Wang, D.; Rus, E. D.; Mundy, J. A.; Muller, D. A.; Abruña, H. D. Three-Dimensional Tracking and Visualization of Hundreds of Pt-Co Fuel Cell Nanocatalysts During Electrochemical Aging. *Nano Lett.* **2012**, *12*, 4417−4423.

(14) Asset, T.; Gommes, C. J.; Drnec, J.; Bordet, P.; Chattot, R.; Martens, I.; Nelayah, J.; Job, N.; Maillard, F.; Dubau, L. Disentangling the Degradation Pathways of Highly Defective PtNi/C Nanostructures − An Operando Wide and Small Angle X-ray Scattering Study. *ACS Catal.* **2019**, *9*, 160−167.

(15) Somorjai, G. A.; Park, J. Y. Molecular surface chemistry by metal single crystals and nanoparticles from vacuum to high pressure. *Chem. Soc. Rev.* **2008**, *37*, 2155−2162.

(16) Somorjai, G. A.; Park, J. Y. Concepts, instruments, and model systems that enabled the rapid evolution of surface science. *Surf. Sci.* **2009**, *603*, 1293−1300.

(17) Kanan, M. W.; Nocera, D. G. In Situ Formation of an Oxygen-Evolving Catalyst in Neutral Water Containing Phosphate and Co^{2+}. *Science* **2008**, *321*, 1072−1075.

(18) Cobo, S.; Heidkamp, J.; Jacques, P.-A.; Fize, J.; Fourmond, V.; Guetaz, L.; Jousselme, B.; Ivanova, V.; Dau, H.; Palacin, S.; Fontecave, M.; Artero, V. A Janus cobalt-based catalytic material for electrosplitting of water. *Nat. Mater.* **2012**, *11*, 802−807.

(19) Bergmann, A.; Martinez-Moreno, E.; Teschner, D.; Chernev, P.; Gliech, M.; de Araújo, J. F.; Reier, T.; Dau, H.; Strasser, P. Reversible amorphization and the catalytically active state of crystalline Co_3O_4 during oxygen evolution. *Nat. Commun.* **2015**, *6*, 8625.

(20) Kim, J.; Noh, M. C.; Doh, W. H.; Park, J. Y. Thermal Evolution and Instability of CO-Induced Platinum Clusters on the Pt(557) Surface at Ambient Pressure. *J. Am. Chem. Soc.* **2016**, *138*, 1110−1113.

(21) Noh, M. C.; Kim, J.; Doh, W. H.; Kim, K. J.; Park, J. Y. Reversible Oxygen-Driven Nickel Oxide Structural Transition on the Nickel(1 1 1) Surface at Near-Ambient Pressure. *ChemCatChem* **2018**, *10*, 2046−2050.

(22) van der Vliet, D. F.; Wang, C.; Li, D.; Paulikas, A. P.; Greeley, J.; Rankin, R. B.; Strmcnik, D.; Tripkovic, D.; Markovic, N. M.; Stamenkovic, V. R. Unique Electrochemical Adsorption Properties of Pt-Skin Surfaces. *Angew. Chem.* **2012**, *124*, 3193−3196.

(23) Kim, J.; Park, W. H.; Doh, W. H.; Lee, S. W.; Noh, M. C.; Gallet, J.-J.; Bournel, F.; Kondoh, H.; Mase, K.; Jung, Y.; Mun, B. S.; Park, J. Y. Adsorbate-driven reactive interfacial Pt-NiO_{1-x} nanostructure formation on the $Pt_3Ni(111)$ alloy surface. *Sci. Adv.* **2018**, *4*, No. eaat3151.

(24) Walton, A. S.; Fester, J.; Bajdich, M.; Arman, M. A.; Osiecki, J.; Knudsen, J.; Vojvodic, A.; Lauritsen, J. V. Interface Controlled Oxidation States in Layered Cobalt Oxide Nanoislands on Gold. *ACS Nano* **2015**, *9*, 2445−2453.

(25) Xin, H. L.; Alayoglu, S.; Tao, R.; Genc, A.; Wang, C.-M.; Kovarik, L.; Stach, E. A.; Wang, L.-W.; Salmeron, M.; Somorjai, G. A.; Zheng, H. Revealing the Atomic Restructuring of Pt−Co Nanoparticles. *Nano Lett.* **2014**, *14*, 3203−3207.

(26) Eren, B.; Salmeron, M. Predicting Surface Clustering at Ambient Conditions from Thermodynamic Data. *J. Phys. Chem. C* **2019**, *123*, 8171−8176.

(27) Ma, Y.; Balbuena, P. B. Pt surface segregation in bimetallic Pt_3M alloys: A density functional theory study. *Surf. Sci.* **2008**, *602*, 107−113.

(28) Lundgren, E.; Stanka, B.; Schmid, M.; Varga, P. Thin films of Co on Pt(111): Strain relaxation and growth. *Phys. Rev. B: Condens. Matter Mater. Phys.* **2000**, *62*, 2843−2851.

(29) Kitchin, J. R.; Nørskov, J. K.; Barteau, M. A.; Chen, J. G. Role of Strain and Ligand Effects in the Modification of the Electronic and

DOI: 10.1021/acsaem.9b01484
ACS Appl. Energy Mater. 2019, 2, 8580−8586

Chemical Properties of Bimetallic Surfaces. *Phys. Rev. Lett.* **2004**, *93*, 156801.
(30) Todorova, M.; Li, W. X.; Ganduglia-Pirovano, M. V.; Stampfl, C.; Reuter, K.; Scheffler, M. Role of Subsurface Oxygen in Oxide Formation at Transition Metal Surfaces. *Phys. Rev. Lett.* **2002**, *89*, 096103.
(31) De Santis, M.; Buchsbaum, A.; Varga, P.; Schmid, M. Growth of ultrathin cobalt oxide films on Pt(111). *Phys. Rev. B: Condens. Matter Mater. Phys.* **2011**, *84*, 125430.
(32) Erlebacher, J. An Atomistic Description of Dealloying: Porosity Evolution, the Critical Potential, and Rate-Limiting Behavior. *J. Electrochem. Soc.* **2004**, *151*, C614−C626.
(33) Chivot, J.; Mendoza, L.; Mansour, C.; Pauporté, T.; Cassir, M. New insight in the behaviour of Co−H_2O system at 25−150°C, based on revised Pourbaix diagrams. *Corros. Sci.* **2008**, *50*, 62−69.
(34) Fester, J.; García-Melchor, M.; Walton, A. S.; Bajdich, M.; Li, Z.; Lammich, L.; Vojvodic, A.; Lauritsen, J. V. Edge reactivity and water-assisted dissociation on cobalt oxide nanoislands. *Nat. Commun.* **2017**, *8*, 14169.
(35) Fester, J.; Sun, Z.; Rodríguez-Fernández, J.; Walton, A. S.; Lauritsen, J. V. Structure and Stability of Au-Supported Layered Cobalt Oxide Nanoislands in Ambient Conditions. *J. Phys. Chem. C* **2019**, *123*, 9176−9182.
(36) Fester, J.; Walton, A.; Li, Z.; Lauritsen, J. V. Gold-supported two-dimensional cobalt oxyhydroxide (CoOOH) and multilayer cobalt oxide islands. *Phys. Chem. Chem. Phys.* **2017**, *19*, 2425−2433.
(37) Petitto, S. C.; Marsh, E. M.; Carson, G. A.; Langell, M. A. Cobalt oxide surface chemistry: The interaction of CoO(100), Co_3O_4(110) and Co_3O_4(111) with oxygen and water. *J. Mol. Catal. A: Chem.* **2008**, *281*, 49−58.
(38) Yang, J.; Liu, H.; Martens, W. N.; Frost, R. L. Synthesis and Characterization of Cobalt Hydroxide, Cobalt Oxyhydroxide, and Cobalt Oxide Nanodiscs. *J. Phys. Chem. C* **2010**, *114*, 111−119.
(39) Biesinger, M. C.; Payne, B. P.; Grosvenor, A. P.; Lau, L. W. M.; Gerson, A. R.; Smart, R. S. C. Resolving surface chemical states in XPS analysis of first row transition metals, oxides and hydroxides: Cr, Mn, Fe, Co and Ni. *Appl. Surf. Sci.* **2011**, *257*, 2717−2730.
(40) Fisher, G. B.; Gland, J. L. The interaction of water with the Pt(111) surface. *Surf. Sci.* **1980**, *94*, 446−455.
(41) Henderson, M. A. The interaction of water with solid surfaces: fundamental aspects revisited. *Surf. Sci. Rep.* **2002**, *46*, 1−308.
(42) Yamamoto, S.; Andersson, K.; Bluhm, H.; Ketteler, G.; Starr, D. E.; Schiros, T.; Ogasawara, H.; Pettersson, L. G. M.; Salmeron, M.; Nilsson, A. Hydroxyl-Induced Wetting of Metals by Water at Near-Ambient Conditions. *J. Phys. Chem. C* **2007**, *111*, 7848−7850.
(43) Yamamoto, S.; Kendelewicz, T.; Newberg, J. T.; Ketteler, G.; Starr, D. E.; Mysak, E. R.; Andersson, K. J.; Ogasawara, H.; Bluhm, H.; Salmeron, M.; Brown, G. E.; Nilsson, A. Water Adsorption on α-Fe_2O_3(0001) at near Ambient Conditions. *J. Phys. Chem. C* **2010**, *114*, 2256−2266.
(44) Kim, K. S. X-ray-photoelectron spectroscopic studies of the electronic structure of CoO. *Phys. Rev. B* **1975**, *11*, 2177−2185.
(45) Weiss, W.; Ranke, W. Surface chemistry and catalysis on well-defined epitaxial iron-oxide layers. *Prog. Surf. Sci.* **2002**, *70*, 1−151.
(46) Fester, J.; Makoveev, A.; Grumelli, D.; Gutzler, R.; Sun, Z.; Rodríguez-Fernández, J.; Kern, K.; Lauritsen, J. V. The Structure of the Cobalt Oxide/Au Catalyst Interface in Electrochemical Water Splitting. *Angew. Chem., Int. Ed.* **2018**, *57*, 11893−11897.
(47) Bajdich, M.; García-Mota, M.; Vojvodic, A.; Nørskov, J. K.; Bell, A. T. Theoretical Investigation of the Activity of Cobalt Oxides for the Electrochemical Oxidation of Water. *J. Am. Chem. Soc.* **2013**, *135*, 13521−13530.
(48) Jiang, C.-M.; Baker, L. R.; Lucas, J. M.; Vura-Weis, J.; Alivisatos, A. P.; Leone, S. R. Characterization of Photo-Induced Charge Transfer and Hot Carrier Relaxation Pathways in Spinel Cobalt Oxide (Co_3O_4). *J. Phys. Chem. C* **2014**, *118*, 22774−22784.
(49) Park, J. Y.; Baker, L. R.; Somorjai, G. A. Role of Hot Electrons and Metal−Oxide Interfaces in Surface Chemistry and Catalytic Reactions. *Chem. Rev.* **2015**, *115*, 2781−2817.
(50) Freund, H.-J. The Surface Science of Catalysis and More, Using Ultrathin Oxide Films as Templates: A Perspective. *J. Am. Chem. Soc.* **2016**, *138*, 8985−8996.

DOI: 10.1021/acsaem.9b01484
ACS Appl. Energy Mater. 2019, 2, 8580−8586